JOURNAL OF MATERIALS SCIENCE **37** (2002) 3053–3057

Interfacial chemistry of powdered barium ferrites immersed in aqueous solutions: leaching in acidic chloride media

S. JACOBO
LAFMACEL, Facultad de Ingeniería, Universidad de Buenos Aires, Paseo Colón 850, 1063-Buenos Aires, Argentina

A. E. REGAZZONI
Unidad de Actividad Química, Centro Atómico Constituyentes, Comisión Nacional de Energía Atómica, Avenida General Paz 1499, 1650-San Martín, Buenos Aires, Argentina

M. A. BLESA*
Unidad de Actividad Química, Centro Atómico Constituyentes, Comisión Nacional de Energía Atómica, Avenida General Paz 1499, 1650-San Martín, Buenos Aires, Argentina; Escuela de Posgrado, Universidad Nacional de General San Martín, Belgrano 3563, 1650 San Martín, Buenos Aires, Argentina
E-mail: miblesa@cnea.gov.ar

The kinetics of leaching and dissolution of barium mono- and hexa-ferrite in acidic chloride media are presented and discussed. The monoferrite is appreciably more reactive, and dissolves in a nearly congruent way in low pH media. In the case of barium hexaferrite, iron and barium dissolution are independent processes. Initially, fast barium leaching is observed, which is followed by a slower process controlled by diffusion through a growing iron oxide layer. Iron dissolves at nearly constant rates that are a function of pH; the apparent kinetic order on H^+ is 0.66, typical of acid dissolution mechanisms. The differing reactivities of the mono- and the hexa-ferrite relates to their crystal chemistry.
© *2002 Kluwer Academic Publishers*

1. Introduction

The search for soft synthetic procedures to prepare oxidic materials is the subject of much current work [1, 2]. Among other advantages, milder procedures, based on the synthesis of intimately mixed, or even homogeneous, precursors, require lower temperatures, and provide a better way to control both particle size and morphology [3, 4]. Even nanosized materials may be prepared by this route.

In this context, the interaction of the oxide particles with aqueous media acquires special importance. Although much work has been devoted to explore the interfacial chemistry of simple oxides immersed in water, much less is known about the nature of the interface in the case of mixed metal oxides [5].

It is well known that barium hexaferrite can be prepared by wet methods, the resulting particles exhibiting very good magnetic properties [6–9]. These procedures work better when some barium excess is used in the synthesis of the precursors to prevent the preferential loss of barium. The excess of barium may result in the formation of detrimental thin surface layers of barium monoferrite, which can be removed by subsequent rinsing with concentrated hydrochloric acid [10, 11]. The evolution of the acid attack, however, is less known. Also, the information related to the possible formation of leached layers and the relative reactivities of $BaFe_{12}O_{19}$ and $BaFe_2O_4$ is scarce. To contribute to the latter subjects, in this paper we explore the mechanism and kinetics of the attack of hydrochloric acid on both barium hexaferrite and barium monoferrite.

2. Experimental

2.1. Sample preparation

Barium hexaferrite was synthesized using the wet procedure described by Ross [7]. The precursor was precipitated upon addition of base to an aqueous solution of Fe^{3+} and Ba^{2+} in a nearly stoichiometric ratio. After drying, the intermediate precipitate was converted into $BaFe_{12}O_{19}$ by heating at 1173 K for 1 h. The XRD pattern of the sample showed only peaks corresponding to the hexaferrite phase. SEM examination showed that the sample was composed of agglomerated microcrystals of different shapes and that most particles were smaller than 5 μm. The specific BET surface area was 5.7 ± 0.6 m^2 g^{-1}.

Barium monoferrite was prepared by the ceramic method, reacting hematite and barium carbonate at

*Author to whom all correspondence should be addressed.

1273 K for 6 h. XRD showed that the sample was composed of the orthorombic variety, mainly; small amounts of the hexagonal phase were also detected [9]. The specific BET surface area was 2.3 ± 0.6 m^2 g^{-1}.

2.2. Kinetic tests

Dissolution experiments were carried out in a magnetically stirred cylindrical glass cell provided with a jacket through which thermostated water (298 ± 0.1 K) was circulated; preliminary experiments showed that rotation speed and type of stirring have no significant effect on dissolution rates. The reaction was started by adding a measured amount of $BaFe_{12}O_{19}$, or $BaFe_2O_4$, to 0.1 dm^3 of a 0.1 mol dm^{-3} KCl solution of fixed pH; the initial surface area concentration was typically 1.7 m^2 dm^{-3}. Throughout the experiments, the pH was kept constant by addition of HCl from a Titrino DMS 716 automatic titrator set in the pH-stat mode. Samples of the suspension were periodically withdrawn, filtered through 0.2 μm cellulose acetate membranes, and stored for analyses. The dissolved iron concentration was determined by measuring the absorbance of the 2,4,6-tripyridil-s-triazineiron(II) complex ($\varepsilon_{593} = 23{,}000$ mol^{-1} dm^3 cm^{-1}) in a Shimadzu UV-210A spectrophotometer. Barium was determined by inductively coupled plasma spectrometry (ICP); the detection limit was 0.1 ppm.

3. Results

3.1. Barium hexaferrite

Figs 1 and 2 show the evolution of dissolved barium and iron during the dissolution of barium hexaferrite at different pH values; note that the data are presented as dissolved fractions, e.g., $f_{Ba} = C_{Ba}/C^T_{Ba}$, where C^T_{Ba} is the concentration of barium at total dissolution. The most obvious feature of Fig. 1 is the large value of 'instantaneously' dissolved barium. This fast initial leaching process is followed by a much slower one, and more than 12 h are required to double the concentration of barium measured at 1 h. On the contrary, the concentration of dissolved iron increases linearly with time (Fig. 2).

These markedly different leaching behaviors indicate that dissolution of $BaFe_{12}O_{19}$ is incongruent. The deviations from stoichiometric dissolution are best exemplified by Fig. 3, which compares the evolution of the dissolved iron to dissolved barium mole ratio at pH 2.4 and 4.0. For congruent dissolution, $n_{Fe}/n_{Ba} = 12$, thus it is concluded that an iron (hydrous)oxide surface layer is left behind by the preferential leaching of barium. In related systems, such layers form even in undersaturated media [12]; note that for pH < 3.4 the dissolution of iron is not limited by the solubility of *am*-Fe(OH)$_3$, i.e., $S > C^T_{Fe}$.

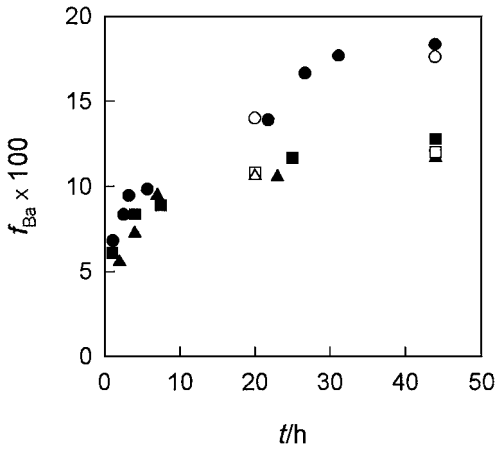

Figure 1 Evolution of barium during the dissolution of barium hexaferrite at pH 2.4 (●), 4.0 (■) and 5.0 (▲); $T = 298$ K. The open symbols correspond to separate runs.

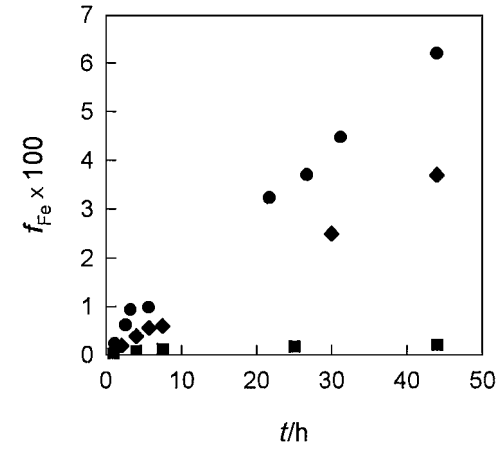

Figure 2 Evolution of iron during the dissolution of barium hexaferrite at pH 2.4 (●), 3.0 (♦) and 4.0 (■); $T = 298$ K.

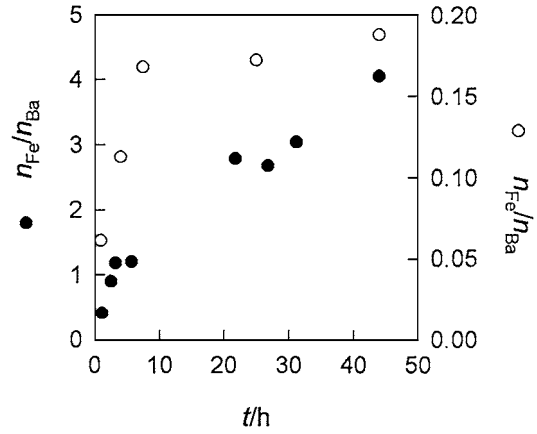

Figure 3 Evolution of the mole ratio of dissolved metals, n_{Fe}/n_{Ba}, during the dissolution of barium hexaferrite at pH 2.4 (●) and 4.0 (○); $T = 298$ K.

Thermodynamically, the concentration of dissolved iron should be limited by the solubility of the most stable crystalline phases. However, reacting solutions are supersaturated with respect to either α-, β- or γ-FeOOH, but undersaturated with respect to *am*-Fe(OH)$_3$ (Fig. 4), a fact that may denote the amorphous nature of the leached surface layer. Attempts to characterize the surface layer by XRD showed hexaferrite only; although these results are inconclusive, they also suggest that the leached layer is amorphous.

The degree of incongruency of the dissolution reaction decreases at the lower pH (Fig. 3). This is a consequence of the different pH dependencies of barium and iron leaching rates. Whereas the pH dependence of the rate of barium dissolution is only modest (Fig. 1), the rate of iron dissolution depends strongly on pH (Fig. 2). From Fig. 5, which shows $R_{Fe,0}$ as a function of pH, a kinetic order on protons of 0.66 is derived.

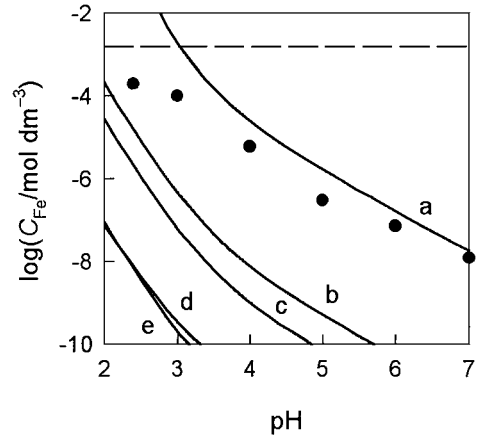

Figure 4 pH dependence of dissolved iron at 44 h (●) Solubilities of ferrihydrite (a), lepidocrocite (b), goethite (c), akaganeite (d) and hematite (e) are also included; they were calculated using the program MINEQL+© ver. 4.0. The horizontal dash line shows C_{Fe}^{T}.

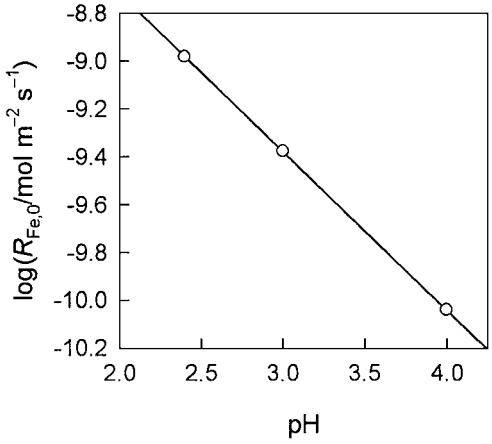

Figure 5 pH dependence of the initial rate of iron dissolution from barium hexaferrite.

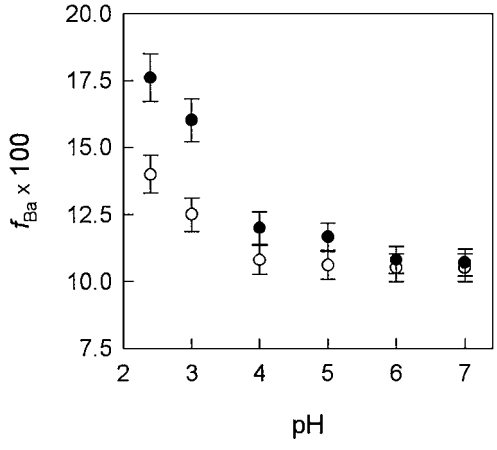

Figure 6 pH dependence of dissolved barium at two fixed times: (○) 20 h; (●) 44 h.

As expected from the solubility of iron (hydrous) oxides, the release of iron above pH 4 is negligible and n_{Fe}/n_{Ba} becomes zero. Under these conditions, the rate of the slower step of barium leaching becomes independent of pH (Fig. 6).

3.2. Barium monoferrite

In the hope to find conditions for congruent behavior, the acid dissolution of barium monoferrite was studied

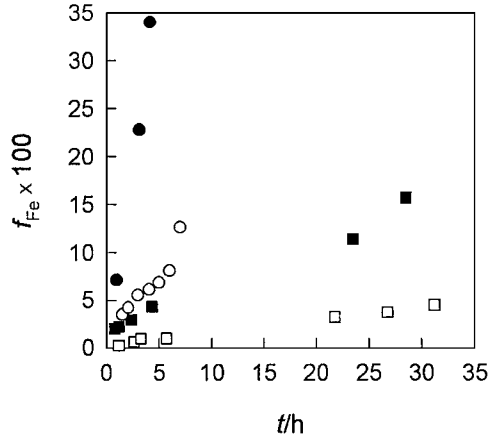

Figure 7 Evolution of iron during the dissolution of barium monoferrite at pH 1.0 (●) and 2.4 (■); $T = 298$ K. The open symbols correspond to barium hexaferrite.

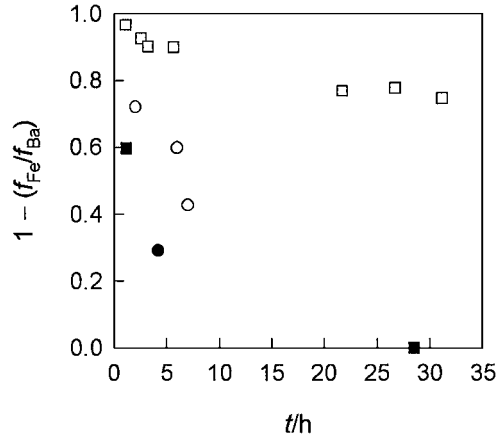

Figure 8 Variation of the degree of incongruency during the dissolution of barium monoferrite (closed symbols) and barium hexaferrite (open symbols) at pH 1.0 (●) and 4.0 (■); $T = 298$ K.

only at pH 2.4 and 1.0. Fig. 7 shows the time profiles of dissolved iron, and Fig. 8 depicts the degree of incongruency, expressed as $[1 - (f_{Fe}/f_{Ba})]$; for congruent dissolution, $[1 - (f_{Fe}/f_{Ba})] = 0$, whereas for barium leaching only, $[1 - (f_{Fe}/f_{Ba})] = 1$. The data indicate that, except for the early stages, the amounts of iron and barium put in solution correspond to a congruent process. For ease of comparison, Figs 7 and 8 include the corresponding data for barium hexaferrite.

Large differences in behavior are apparent: (i) the dissolution of $BaFe_2O_4$ is roughly congruent, whereas $BaFe_{12}O_{19}$ dissolution is largely incongruent. (ii) the amounts of dissolved metals are appreciably larger for the monoferrite; for $BaFe_2O_4$, $R_{Fe,0}$ is about six times larger. (iii) for the monoferrite, and also for the hexaferrite at pH 1.0, the f_{Fe} vs. t profiles are not linear, a likely consequence of a complex evolution of particle size and morphology [5].

4. Discussion

The interaction of mixed oxides formed from a sparingly soluble one (α-Fe_2O_3) and a largely soluble one (BaO) with aqueous solutions can be described as [13],

$$BaFe_{12}O_{19}(s) + 38H^+ \rightarrow Ba^{2+} + 6Fe^{3+} + 19H_2O \quad (1)$$

$$BaFe_{12}O_{19}(s) + 2H^+ \rightarrow Ba^{2+} + 6Fe_2O_3(s) + H_2O \quad (2)$$

Similar reactions can be written for $BaFe_2O_4$. Whether stoichiometric dissolution (Equation 1) or phase transformation (Equation 2) takes place, depends on the pH dependent solubility of the iron oxide. Of course, the overall behavior is determined by the actual stability of the ferrite. The available thermodynamic information on barium hexaferrite refers to temperatures above 860 K [14–16]. Furthermore, the data sets are appreciably different; extrapolation to 298 K using the simple proposed $\Delta G_3^0(T)$ expression leads to $\Delta G_3^0(298)$ values that range from 80 to 340 kJ mol^{-1}.

$$BaFe_{12}O_{19}(s) = BaO(s) + 6Fe_2O_3(s) \quad (3)$$

These figures do not permit the estimation of the equilibrium constants for reactions (1) and (2); for reaction (2), $\Delta G_2^0(298)$ values range from -200 to $+75$ kJ mol^{-1}. Our data, however, demonstrate that the behavior of barium hexaferrite is similar to that of other related mixed oxides [12, 13]; i.e., leaching of barium is spontaneous. Similar considerations apply to barium monoferrite, for which $\Delta G_{2'}^0(298) \approx -190$ kJ mol^{-1} [14–16].

Phase transformation does not necessarily takes place as depicted by Equation 2, which represents the most stringent thermodynamic constraint for both iron and barium dissolution, and other less stable iron (hydrous)oxides may form, as seems to be the present case (Fig. 4). Formation of *am*-$Ti(OH)_4$ on the surface of dissolving titanates is well documented [12, 17]. The operating overall dissolution-reprecipitation mechanism should therefore determine the nature of the leached surface layer.

The general mechanism describing the acid attack of the barium ferrites must involve the following stages [5, 17]:

(i) Proton adsorption and ionic exchange, as represented by Equations 4 and 5:

$$\equiv Fe\text{-}OH + H^+ \rightarrow \equiv Fe\text{-}OH_2^+ \quad (4)$$

$$\equiv Ba^{2+} + 2H^+ \rightarrow 2 \equiv H^+ + Ba^{2+} \quad (5)$$

Equation 4 describes a well-known property of oxide materials immersed in water; the symbol $\equiv$ represents the bonds linking the given surface species to the solid framework. Surface protonation is a common prerequisite for acid dissolution [5, 18, 19]. The ionic exchange reaction (5) accounts for the fast release of barium in the time span within which iron dissolution is comparatively negligible (cf., Figs 1 and 2). The net result in this early step is the creation of an iron-rich layer that participates in the following stages of the dissolution reaction; on the basis of the amount of barium released 'instantaneously' (within 1 h), the thickness of the iron rich layer is calculated to be ca. 15 nm.

(ii) Iron dissolution from the outer surface of the external layer, coupled with barium diffusion across this layer and dissolution:

$$\equiv Fe^{3+} \rightarrow Fe^{3+}; \quad R_{Fe} \quad (6)$$

$$\equiv Ba^{2+} \rightarrow Ba^{2+}; \quad R_{Ba} \quad (7)$$

At low (constant) pH values, the rate of iron dissolution R_{Fe} is constant (see Fig. 2), as expected for a constant surface area in a medium of constant aggressivity; the low pH value suffices to define this latter condition. As opposed to well known cases in which the dissolved ions influence the rate of dissolution [5], released Fe(III) and Ba^{2+} do not alter the constant rate of iron dissolution. Note that the fraction of dissolved iron does not exceed 7%, thus the assumption of constant surface area is valid. At pH 1.0, the evolution of the attack front is more complex (Fig. 7).

The lack of congruency determines that 12 $R_{Ba} > R_{Fe}$. Consequently, the thickness of the iron oxide layer grows during dissolution. This should lead to parabolic f_{Ba} vs. t profiles. The fact that barium concentration grows almost linearly with the square root of time, albeit with a non-zero ordinate (Fig. 9B), indicates that the leaching of barium is controlled by diffusion through a growing insoluble layer. A more adequate treatment, however, must take into account the amount of barium dissolved during the first stage (Equation 5). Assuming that the barium dissolved in the first stage, which accounts for that dissolved in the first hour, follows first order kinetics on exchangeable barium [20], the time dependence of f_{Ba} can be written as,

$$f_{Ba} = N_0[1 - \exp(-k_0 t)] + k_D t^{0.5} \quad (8)$$

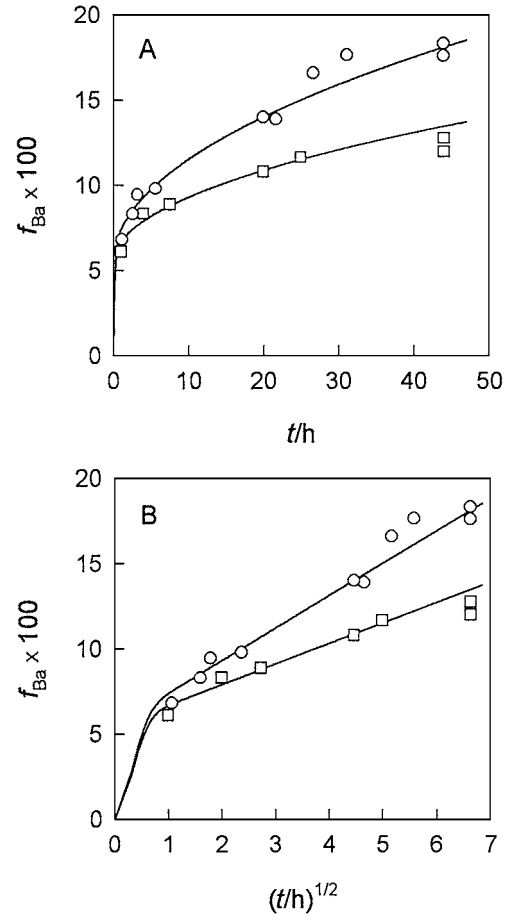

Figure 9 Evolution of barium during the dissolution of barium hexaferrite as predicted by Equation 8; symbols are the actual data points collected at pH 2.4 (○) and 4.0 (□). The following rate parameters define the solid lines: $N_0 = 0.055$; $k_0 = 5$ h^{-1}; $k_D = 0.019$ h$^{-0.5}$ (for pH 2.4) and $k_D = 0.012$ h$^{-0.5}$ (for pH 4.0).

where N_0 is the total fraction of exchangeable barium, and k_0 and k_D are the rate constants for the first and second stages, respectively. The goodness of the fittings is shown in Fig. 9. The compliance of the second stage to a parabolic law (Fig. 9B) is, however, at variance with the non-negligible dissolution of the iron oxide layer (Fig. 2), especially for pH 2.4 where the degree of congruency is larger (Fig. 3). It must be concluded that the effect of the decreased thickness of the iron oxide layer at pH 2.4 is roughly compensated by changes, possibly crystallization, that make it less permeable.

The low barium content of $BaFe_{12}O_{19}$ is probably associated with a very modest enhancement in the dissolution rate of iron from the hexaferrite, as compared with pure iron oxides. The leaching of barium creates vicinal sites of increased reactivity [5, 21], but the block structure of the hexaferrite probably defines that the rates of iron dissolution are determined by the reactivity of the barium-free blocks that are similar in structure to hematite; note that the fractional kinetic order on protons (Fig. 5) is typical of iron oxides [5]. By contrast, barium monoferrite has a Ba : Fe mole ratio of 0.5, and does not present iron-only blocks. Its reactivity is therefore higher, and furthermore it dissolves in a more congruent fashion (Fig. 8). This increased reactivity is put to use in the acid-rinsing of industrial batches of barium hexaferrite, to improve the magnetic properties.

Acknowledgments

Supported by CNEA, and by Grants PIP 4196/96 from CONICET, PICT 306/97 from ANPCYT, and EX 036 from UBA. AER and MAB are members of CONICET.

References

1. C. J. BRINKER and G. W. SCHERER, "Sol-Gel Science" (Academic Press, New York, 1990).
2. L. V. INTERRANTE and M. J. HAMPDEN-SMITH (eds.), "Chemistry of Advanced Materials: An Overview" (Wiley, New York, 1998).
3. E. MATIJEVIĆ, in "Untrastructure Processing of Advanced Ceramics," edited by S. D. MacKenzie and D. R. Ulrich (Wiley, New York, 1988) p. 429.
4. *Idem.*, in "Chemical Processing of Advanced Materials," edited by L. H. Hench and J. K. West (Wiley, New York, 1992) p. 513.
5. M. A. BLESA, P. J. MORANDO and A. E. REGAZZONI, "Chemical Dissolution of Metal Oxides" (CRC Press, Boca Raton, FL, 1994).
6. W. ROSS, *J. Amer. Ceram. Soc.* **53** (1969) 192.
7. *Idem.*, *ibid.* **63** (1980) 601.
8. S. E. JACOBO and M. A. BLESA, *J. Phys. Fr.* IV **7** (1997) C1-319.
9. S. E. JACOBO, Ph.D. Diss., FECN, UBA, Argentina, 1998.
10. M. RÖSLER, P. GÖRNERT and E. SINN, *Z. Phys.* D **19** (1991) 279.
11. K. HANEDA and H. KOJIMA, *J. Appl. Phys.* **44** (1973) 3760.
12. J. A. SALFITY, A. E. REGAZZONI and M. A. BLESA, in 5th Southern Hemisphere Meeting on Mineral Technology, INTEMIN, Buenos Aires, Argentina, 1997, p. 185.
13. M. A. BLESA, G. J. DE AA. SOLER-ILLIA, R. J. CANDAL and A. E. REGAZZONI, in "Fine Particles Science and Technology," edited by E. Pelizzetti (Kluwer, Dordrecht, 1996) p. 33.
14. B. DEO, J. S. KACHHAWAHA and V. B. TARE, *Metall. Trans.* B **7B** (1976) 405.
15. G. POUILLARD, M. S. ALAM, M.-C. TRINEL-DUFOUR and P. PERROT, *J. Chem. Res.* (S) **136** (1981) 136.
16. J. LI, T. M. GÜR, M. SINCLAIR, S. S. ROSENBLUM and H. HAYASHI, *J. Mater. Res.* **9** (1994) 1499.
17. P. S. TURNER, C. F. JONES, S. MYHRA, F. B. NEALL, D. K. PHAM and R. ST. C. SMART, in "Surfaces and Interfaces of Ceramic Materials," edited by L.-C. Dufour, C. Monty and G. Petot-Ervas (Kluwer, Dordrecht, 1989) p. 663.
18. E. WIELAND, B. WEHRLI and W. STUMM, *Geochim. Cosmochim. Acta* **52** (1988) 1969.
19. M. A. BLESA, A. D. WEISZ, P. J. MORANDO, J. A. SALFITY, G. E. MAGAZ and A. E. REGAZZONI, *Coord. Chem. Rev.* **196** (2000) 31.
20. J. A. SALFITY, A. E. REGAZZONI and M. A. BLESA, unpublished.
21. C. A. FIGUEROA, E. E. SILEO, P. J. MORANDO and M. A. BLESA, *J. Colloid Interface Sci.* **225** (2000) 403.

Received 12 January 2001
and accepted 9 April 2002